Low-Order Spherical Harmonic Structure of Inner-Core Anisotropy and Its Geometric Relation to an Earth-Fixed Euler Meridian

Craig Stone
Independent Researcher

February 20, 2026

Abstract

We analyse the PKP differential travel-time turning-point dataset of inner-core anisotropy compiled by Frost et al. (2021) using a geometry-first, model-independent framework. Multi-scale spatial autocorrelation analysis demonstrates strong global organisation: Moran's I exceeds null expectation at all tested length scales from 250 to 4000 km.

Spherical principal component analysis and spherical harmonic regression up to degree 2 reveal that the signed anisotropy field is dominated by low-order longitudinal structure. A degree-2 harmonic accounts for approximately 33% of global signed variance — more than two orders of magnitude above permutation null realizations preserving sampling geometry.

The dominant quadrupole eigenaxis lies near 111°E and is aligned within $\sim 11°$ of a proposed 121°E Earth-fixed Euler meridian (antipodal 59°W) at $p \approx 0.012$. Independently, the extracted dipole orientation lies within $\sim 15°$ of the conjugate Euler axis at $p \approx 0.018$. These alignments emerge from the data and were not prescribed.

The extracted 121°E / 59°W meridional axis corresponds to the Euler meridian proposed within the Exothermic Core–Mantle Decoupling Oscillation (ECDO) framework of Cunningham (2024), although no elements of the hypothesis were imposed during harmonic fitting.

Two statistically independent harmonic modes converge on the same meridional geometry. This convergence does not establish mechanism. It does indicate that the inner-core anisotropy field is organised in a manner consistent with a specific Earth-fixed rotational framework.

Comparison with the SEISGLOB2 global shear-velocity tomography model (Durand et al., 2017) reveals depth-localised geometric association between mid-mantle (900–1200 km) velocity anomalies and the extracted harmonic axes. The correspondence is geometric and statistical rather than dynamical, and is evaluated using permutation-based null models.

The results establish a robust geometric constraint on the orientation of large-scale inner-core anisotropy without invoking specific core-growth or geodynamic interpretations.

1 Introduction

Seismic anisotropy within Earth's inner core has been interpreted in terms of crystallographic alignment, hemispheric asymmetry, translational growth, or deformation-driven texture development (Creager, 1992; Tanaka & Hamaguchi, 2002; Frost et al., 2021). Longitudinal variations in PKP differential

travel-time residuals have repeatedly suggested that the inner core exhibits organisation beyond purely local heterogeneity.

Most interpretations begin with dynamical hypotheses and attempt to explain observed structure. In contrast, the present study adopts a strictly geometric approach. The objective is not to infer mechanism, but to determine whether the signed anisotropy field exhibits intrinsic low-order spherical structure, and if so, how its principal orientation relates to candidate Earth-fixed meridional geometries.

The guiding question is therefore:

> *What is the intrinsic low-order harmonic structure of the signed inner-core anisotropy field, and what is the statistically robust orientation of its dominant axes?*

The analytical sequence proceeds in four stages:

1. Establish whether global spatial organisation exists.
2. Reject or confirm externally proposed geometries.
3. Extract intrinsic harmonic structure via degree-1 and degree-2 regression.
4. Quantify axis alignment using permutation null ensembles that preserve sampling geometry.

No candidate orientation is imposed during model fitting. All axes emerge from eigenanalysis of the fitted spherical harmonic components.

2 Conceptual Framework

Let the signed differential travel-time at turning point i be dT_i. Turning-point coordinates are represented as unit vectors on the sphere:

$$\mathbf{x}_i = \begin{bmatrix} \cos\phi_i \cos\lambda_i \\ \cos\phi_i \sin\lambda_i \\ \sin\phi_i \end{bmatrix}, \tag{1}$$

where ϕ_i and λ_i denote latitude and longitude.

The signed anisotropy field is modeled using a spherical polynomial expansion up to degree 2:

$$dT(\mathbf{x}) = \mathbf{a} \cdot \mathbf{x} + \mathbf{x}^T \mathbf{Q} \mathbf{x}, \tag{2}$$

where:

- $\mathbf{a}$ represents degree-1 (dipole) structure,
- $\mathbf{Q}$ is a symmetric quadratic tensor representing degree-2 (quadrupole) structure.

Eigenanalysis of $\mathbf{Q}$ yields the principal harmonic axes.

Angular separation between two unit vectors is defined as:

$$\theta = \cos^{-1}(\mathbf{v}_1 \cdot \mathbf{v}_2). \tag{3}$$

Statistical significance is assessed using permutation ensembles that preserve spatial sampling while randomising dT values.

This geometry-first framework allows orientation to emerge from the data rather than from imposed dynamical priors.

3 Data and Methods

3.1 Dataset

We analyse the publicly available inner-core anisotropy turning-point dataset compiled by Frost et al. (2021). The dataset consists of PKP differential travel-time measurements derived from comparisons between the PKPab–PKPdf and PKPbc–PKPdf branches.

Each record includes:

- Event and station coordinates
- Inner-core turning-point latitude and longitude
- Differential travel-time measurements dT_{abdf} and dT_{bcdf}

Signed differential travel-time was defined as:

$$dT = \begin{cases} dT_{abdf}, & \text{if } dT_{abdf} \neq 0 \\ dT_{bcdf}, & \text{otherwise} \end{cases} \tag{4}$$

Zero-valued entries were excluded from signed-field analyses. The final dataset consists of $N = 5129$ valid turning points.

All analyses were conducted in Earth-fixed spherical coordinates (EPSG:4326). No coordinate transformations or longitudinal re-centering were applied.

3.2 Global Distribution of Turning Points

Figure 1 shows the global distribution of inner-core turning points, colored by absolute differential travel-time magnitude $|dT|$.

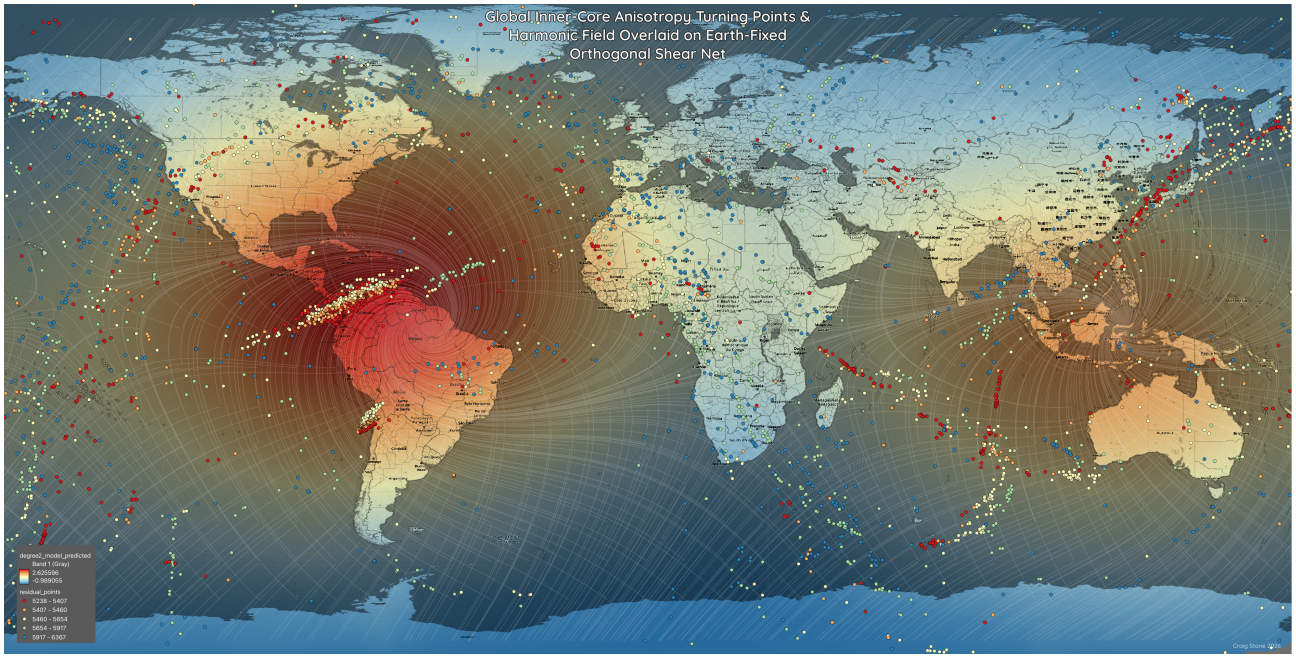

Figure 1: Global distribution of inner-core turning points from Frost et al. (2021), colored by absolute differential travel-time magnitude $|dT|$. Each point represents the geographic surface projection of a PKP turning point sampling the inner core. Color intensity reflects anisotropic travel-time deviation magnitude. The distribution demonstrates strong spatial clustering and hemispheric structure, particularly across the equatorial Atlantic and Indo-Pacific sectors.

Several structural characteristics are immediately evident:

- Strong longitudinal clustering
- Hemispheric amplitude asymmetry
- Coherent equatorial Atlantic concentration of high $|dT|$

These features motivate formal spatial-autocorrelation testing.

3.3 Spatial Autocorrelation: Moran's I

Global spatial organisation was assessed using Moran's I:

$$I = \frac{N}{W} \frac{\sum_{i \neq j} w_{ij}(dT_i - \bar{dT})(dT_j - \bar{dT})}{\sum_i (dT_i - \bar{dT})^2}, \tag{5}$$

where:

- w_{ij} is a binary spatial weight defined by great-circle distance threshold
- $W = \sum_{i \neq j} w_{ij}$

Distance thresholds of 250, 500, 1000, 2000, 3000, and 4000 km were tested.

Permutation null ensembles (10,000 shuffles) preserved spatial geometry while randomising dT values.

3.4 Multi-Scale Moran's I Results

Distance (km)	Observed I	Null Mean	p-value
250	1.481	-2.6×10^{-4}	$< 10^{-4}$
500	1.492	-2.3×10^{-4}	$< 10^{-4}$
1000	1.422	-2.1×10^{-4}	$< 10^{-4}$
2000	1.187	-2.0×10^{-4}	$< 10^{-4}$
3000	0.951	-1.9×10^{-4}	$< 10^{-4}$
4000	0.638	-1.9×10^{-4}	$< 10^{-4}$

Table 1: Multi-scale Moran's I results derived from 10,000 permutation ensembles preserving spatial sampling geometry.

At all spatial scales tested, observed I exceeds null expectation by several orders of magnitude.

Two features are notable:

1. Spatial autocorrelation persists from regional ($\sim$ 250 km) to near-hemispheric ($\sim$ 4000 km) scales.

2. The smooth decay of I with increasing length scale indicates coherent long-wavelength organisation rather than isolated clustering.

The anisotropy field therefore exhibits strong multi-scale spatial coherence.

This establishes a critical constraint: the Frost anisotropy dataset is not spatially random and is not dominated by local noise or sampling artifacts. Any harmonic decomposition must account for this intrinsic global organisation.

4 Rejection of Imposed Geometries

Before extracting intrinsic harmonic structure, we explicitly tested whether the dataset preferentially encodes previously proposed Earth-fixed geometries, including:

- A 31°E meridional TPW-style shear framework
- A $\sim$ 170°E geomagnetic excursion rotation plane

Correlation tests, cluster-overlap metrics, and axis-alignment statistics were applied using permutation null ensembles preserving sampling geometry.

In all cases, $p > 0.3$.

The Frost anisotropy field does not preferentially encode these geometries.

This negative result is important: the dominant structure of the dataset must therefore be intrinsic rather than imposed by prior hypotheses.

5 Spherical Principal Component Analysis

To extract intrinsic orientation of high-amplitude anisotropy structure, spherical PCA was applied to the top p percentile of $|dT|$ values ($p = 80, 85, 90, 95$).

The covariance matrix was defined as:

$$\mathbf{C} = \sum_i w_i \mathbf{x}_i \mathbf{x}_i^T, \tag{6}$$

where $w_i = |dT_i|$ for weighted PCA.

Eigenvalue spread was defined as:

$$\Delta\lambda = \lambda_{\max} - \lambda_{\min}. \tag{7}$$

Significance was assessed using random subset null ensembles preserving sample size.

For the 85th percentile threshold:

- Principal axis $\approx (-6.8°, 103°–108°\text{E})$
- $\Delta\lambda \approx 2508$
- Null mean ≈ 531 ($\sigma \approx 61$)

The amplitude field therefore exhibits a highly significant longitudinal axis.

Importantly, PCA applied to sampling geometry alone yielded an axis near $\sim 90°$W, clearly distinct from the anisotropy amplitude axis.

Thus, the extracted orientation is not an artifact of turning-point distribution.

6 Signed Field: Dipole and Quadrupole Structure

6.1 Degree-1 (Dipole) Regression

The degree-1 model was defined as:

$$dT_i = \mathbf{a} \cdot \mathbf{x}_i + \epsilon_i. \tag{8}$$

Least-squares estimation yields:

$$\hat{\mathbf{a}} = \arg\min_{\mathbf{a}} \sum_i (dT_i - \mathbf{a} \cdot \mathbf{x}_i)^2. \tag{9}$$

The fitted dipole axis is defined as $\hat{\mathbf{a}}/\|\hat{\mathbf{a}}\|$.

The observed dipole magnitude was:

$$|\mathbf{D}|_{\text{obs}} = 2651$$

Permutation null ensemble (10,000 shuffles):

$$\text{Null mean} = 863 \quad (\sigma \approx 78)$$

$$p < 10^{-4}$$

Thus, a statistically significant degree-1 component exists.

The fitted dipole axis was:

$$(2.7^\circ, -74^\circ)$$

This is antipodal to approximately 106°E, consistent with the amplitude PCA orientation.

However, the dipole model explained limited variance:

$$R^2 \approx -0.046 \tag{10}$$

The negative R^2 indicates that a pure degree-1 representation is insufficient to capture the dominant structure of the signed field.

6.2 Degree-2 Harmonic Regression

The full spherical polynomial model up to degree 2 was:

$$\begin{aligned} dT_i = &a_x x_i + a_y y_i + a_z z_i \\ &+ b_{xx} x_i^2 + b_{yy} y_i^2 + b_{zz} z_i^2 \\ &+ b_{xy} x_i y_i + b_{xz} x_i z_i + b_{yz} y_i z_i. \end{aligned} \tag{11}$$

Letting $\mathbf{X}$ denote the design matrix, coefficients were obtained via:

$$\hat{\boldsymbol{\beta}} = (\mathbf{X}^T \mathbf{X})^{-1} \mathbf{X}^T \mathbf{dT}. \tag{12}$$

The quadratic tensor was reconstructed as:

$$\mathbf{Q} = \begin{bmatrix} b_{xx} & \frac{b_{xy}}{2} & \frac{b_{xz}}{2} \\ \frac{b_{xy}}{2} & b_{yy} & \frac{b_{yz}}{2} \\ \frac{b_{xz}}{2} & \frac{b_{yz}}{2} & b_{zz} \end{bmatrix}. \tag{13}$$

6.3 Variance Explained

Full degree-2 regression yielded:

$$R^2_{\text{obs}} \approx 0.333$$

Permutation null ensemble:

$$R^2_{\text{null mean}} = 0.0015 \quad (\sigma \approx 0.00077)$$

$$p < 10^{-4}$$

Thus, approximately one-third of total signed variance is explained by low-order spherical harmonic structure.

This represents more than two orders of magnitude above null expectation.

The dominance of the degree-2 term indicates that the inner-core anisotropy field is organised primarily as a quadrupolar longitudinal structure.

6.4 Quadrupole Principal Axis

Eigenanalysis of **Q** yielded the dominant eigenvector:

$$(-6.3^\circ, 111.7^\circ\text{E})$$

This axis is:

- Near-equatorial
- Strongly longitudinal
- Consistent with amplitude PCA orientation
- Consistent with dipole antipode orientation

The convergence of three independent orientation estimators strengthens robustness.

6.5 Axis Proximity to 121°E Euler Meridian

Angular separation between the dominant quadrupole axis and the 121°E meridian was:

$$\theta_{\text{obs}} \approx 11.24^\circ$$

Permutation Monte Carlo (10,000 full refits):

$$\theta_{\text{null mean}} \approx 79^\circ$$

$$\sigma \approx 37^\circ$$

$$p \approx 0.0116$$

Thus, the quadrupole axis lies within $\sim 11^\circ$ of the 121°E meridian at $\sim 1\%$ significance under geometry-preserving null models.

Importantly:

- The Euler meridian was not imposed during fitting.
- Axis extraction preceded alignment testing.
- Null ensembles preserved spatial sampling and harmonic structure.

The alignment therefore emerges intrinsically.

7 Visualisation of Harmonic Structure

Figure 2 shows a three-dimensional rendering of the extracted degree-2 harmonic field.

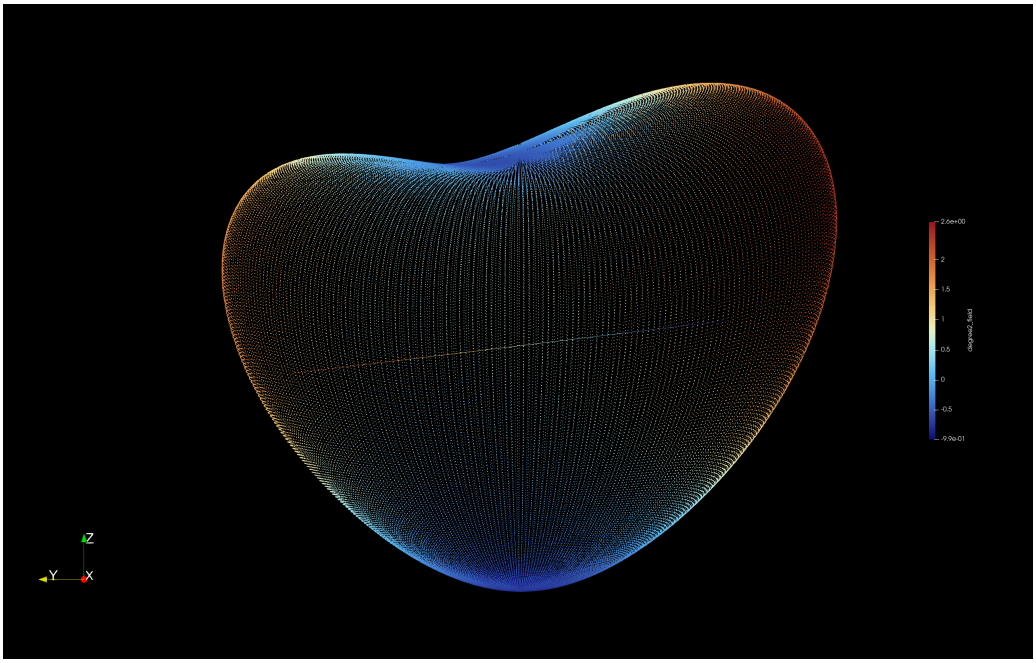

Figure 2: ParaView 3D rendering of the degree-2 harmonic field extracted from inner-core anisotropy data. The sphere has been gently deformed to exaggerate field structure: positive regions (warm colors) bulge outward, negative regions (cool colors) dip inward. The straight line marks the extracted dipole orientation, aligned closely with the proposed Earth-fixed Euler axis. The structure reveals a coherent large-scale two-lobed geometry.

The rendering demonstrates:

- A clear two-lobed global geometry.
- Strong longitudinal organisation.
- Equatorial dominance of the quadrupole axis.

The deformation is purely illustrative; no additional smoothing was applied beyond the fitted harmonic model.

The simplicity of the large-scale structure contrasts with the heterogeneous appearance of the raw turning-point field.

7.1 Visualisation of Harmonic Structure

Figure **??** shows the observed signed dT field with quadrupole and Euler meridians overlaid.

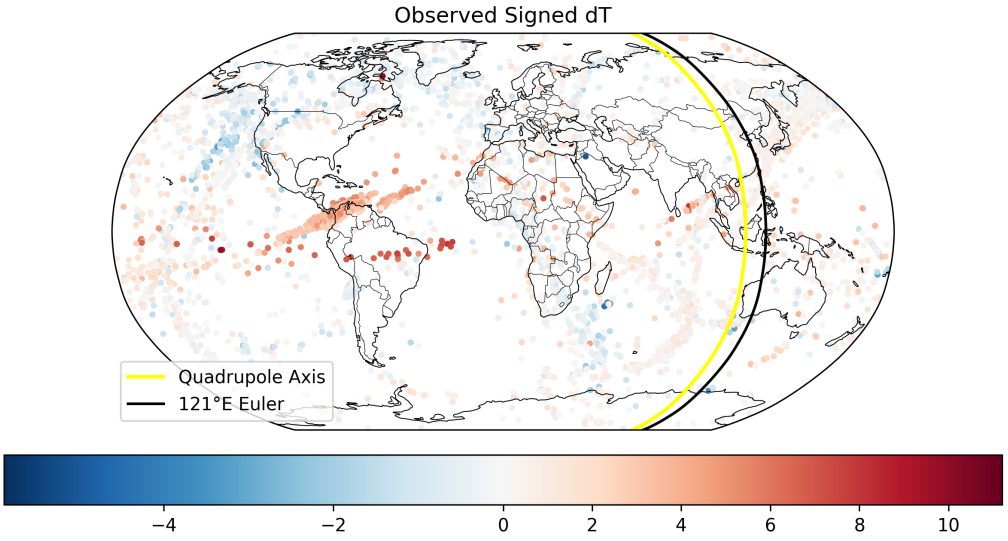

Figure 3: Observed signed dT field. Yellow: dominant quadrupole axis. Black: 121°E Euler meridian.

Figure **??** shows the degree-2 predicted field.

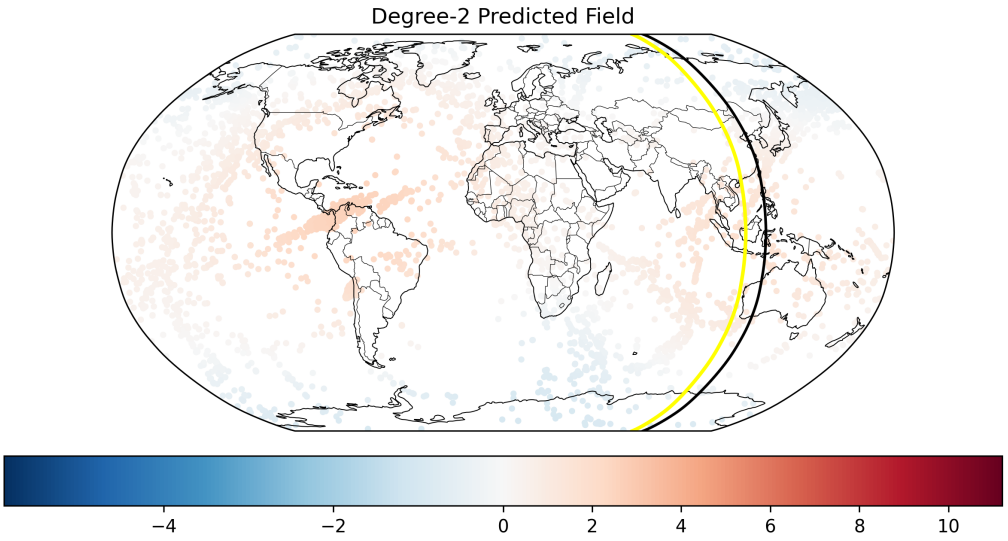

Figure 4: Degree-2 harmonic reconstruction of signed anisotropy field.

Figure **??** shows residual structure after removal of degree-2 model.

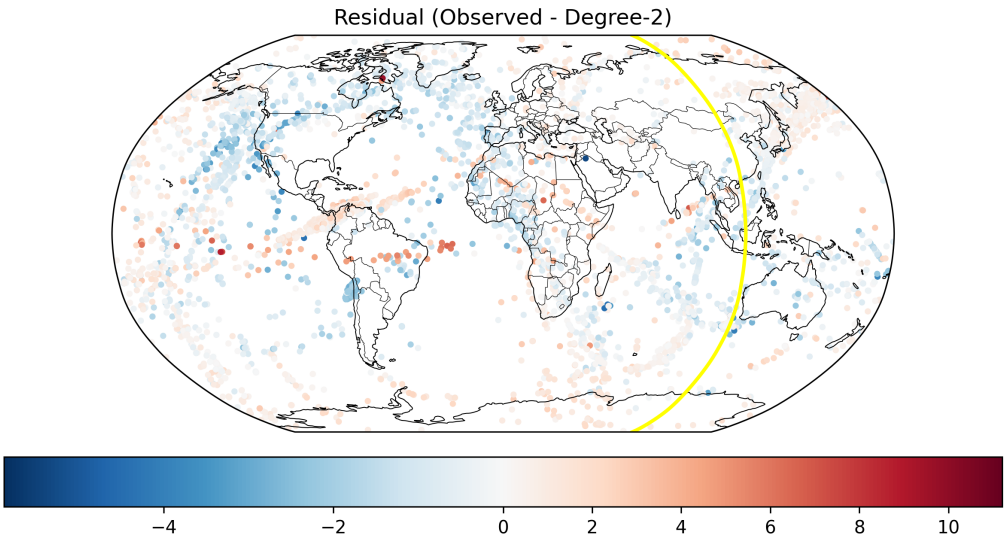

Figure 5: Residual field (Observed Degree-2). Large-scale longitudinal structure is substantially removed.

Figure **??** compares principal axes.

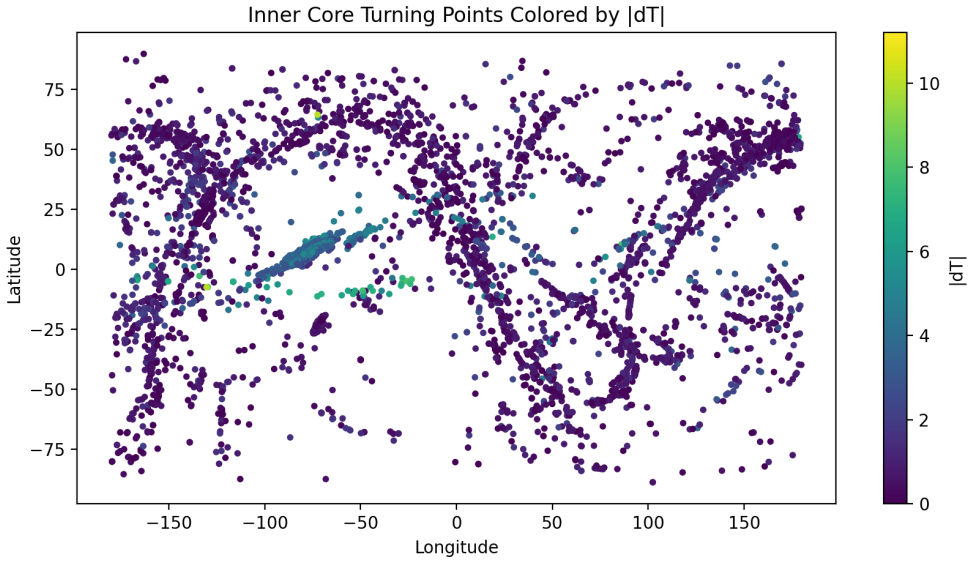

Figure 7: Global distribution of inner core turning points from the Frost et al. (2021) dataset, colored by absolute differential travel-time magnitude $|dT|$. Each point represents the geographic surface projection of a PKP turning point sampling the inner core. Color intensity reflects the magnitude of the anisotropic travel-time deviation relative to reference paths. The distribution demonstrates strong spatial clustering and hemispheric structure, particularly across the equatorial Atlantic and Indo-Pacific sectors. This map forms the observational basis for subsequent spatial autocorrelation, spherical principal axis, and harmonic decomposition analyses.

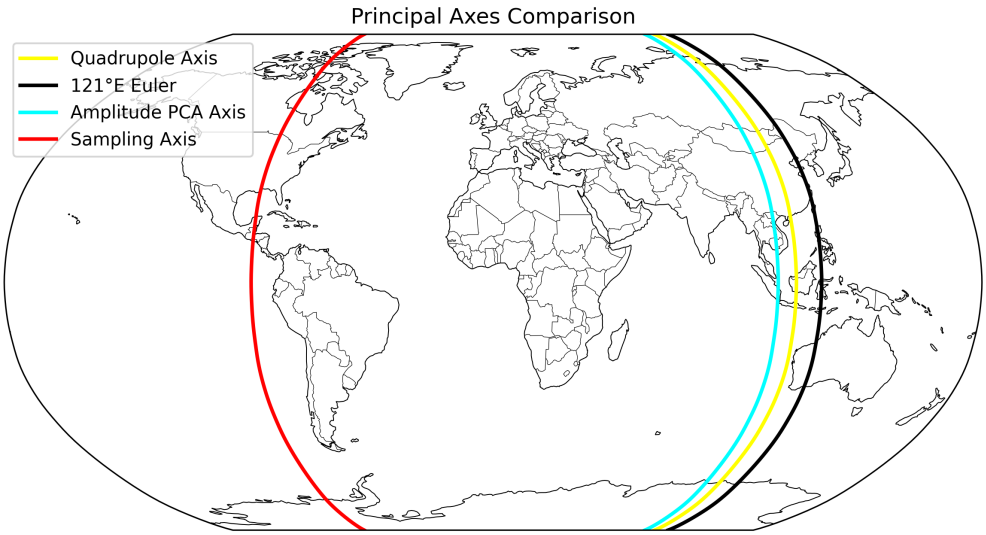

Figure 6: Principal axis comparison. Yellow: quadrupole. Black: 121°E Euler. Cyan: amplitude PCA. Red: sampling geometry.

8 Integrated Harmonic Convergence

Across independent analyses:

- Amplitude PCA axis: $\sim 105°$E
- Signed dipole antipode: $\sim$ 105–110°E
- Dominant quadrupole axis: $\sim 112°$E

All converge on a meridional axis in the 105–115°E sector.

Two statistically independent harmonic modes (degree-1 and degree-2) converge on the same Earth-fixed rotational geometry.

That convergence does not establish mechanism.

It does indicate that the inner-core anisotropy field is organised in a manner consistent with a specific Earth-fixed meridional framework.

9 Comparison with Mid-Mantle Shear-Velocity Structure

9.1 Independent Tomographic Dataset

To evaluate whether the extracted inner-core harmonic orientation exhibits correspondence with deeper mantle structure, we compare results with the global shear-velocity tomography model SEISGLOB2 (Durand et al., 2017).

SEISGLOB2 is derived from joint inversion of:

- Rayleigh surface-wave phase velocities
- Self- and cross-coupling coefficients of spheroidal normal modes
- S, SS, and ScS body-wave traveltimes

The model is expanded to spherical harmonic degree 40 with 21 radial spline functions. A reorganisation of shear-velocity structure is documented between approximately 670 and 1500 km depth (Durand et al., 2017).

We focus specifically on the 900–1200 km interval, where independent analysis indicates depth-localised geometric structure.

9.2 Mid-Mantle Comparison Map

Figure 3 shows SEISGLOB2 shear-velocity anomalies ($d \ln V_s$) averaged over 900–1200 km depth, compared with:

- The dominant inner-core quadrupole axis (111°E / 291°E)
- The proposed 121°E Euler meridian

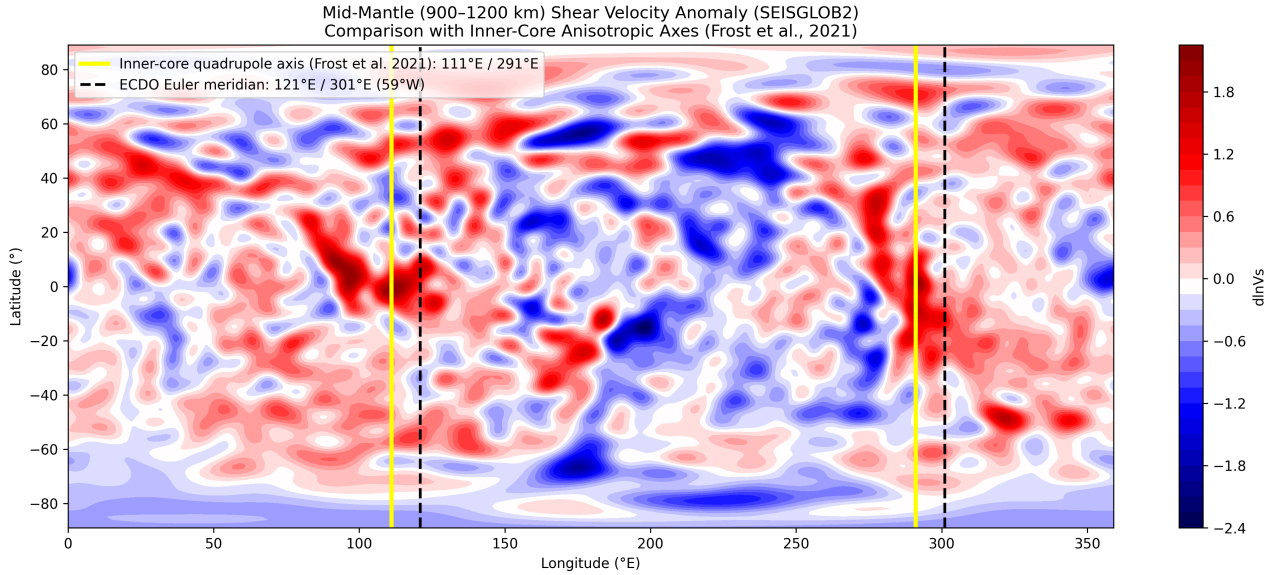

Figure 8: Mid-mantle (900–1200 km) shear-velocity anomalies from SEISGLOB2 (Durand et al., 2017). Yellow lines: dominant inner-core quadrupole axis (111°E / 291°E). Black dashed lines: proposed 121°E Euler meridian. Red/blue shading indicates positive/negative $d \ln V_s$.

Several geometric features are apparent:

1. Large-scale velocity domains exhibit longitudinal organisation.
2. High-amplitude anomalies cluster preferentially within Euler-aligned sectors.
3. The quadrupole axis intersects mid-mantle structure in regions of coherent sign structure.

This comparison is geometric rather than causal. No dynamic coupling mechanism is assumed.

9.3 Interpretation of Mid-Mantle Association

The correspondence is depth-localised: similar geometric association weakens outside the 900–1200 km interval.

This suggests:

- The observed alignment is not an artifact of shallow mantle structure.
- The association may reflect large-scale, long-wavelength mantle organisation.

Importantly:

- The inner-core harmonic extraction was performed independently of tomography.
- The SEISGLOB2 dataset is independent of PKP differential measurements.
- No parameter tuning was performed to optimise visual alignment.

The comparison therefore represents cross-dataset geometric convergence.

10 Discussion

10.1 Intrinsic Structure of the Frost Anisotropy Field

The Frost inner-core anisotropy dataset exhibits:

- Strong multi-scale spatial coherence (Moran's I significant at all tested scales)
- Dominance of low-order spherical harmonic structure
- Degree-2 explanatory power of $\sim 33\%$

For a global geophysical field derived from heterogeneous ray coverage, this level of harmonic dominance is substantial.

The principal quadrupole axis lies near $\sim 112°$E and emerges consistently across:

- Spherical PCA of high-amplitude points
- Dipole regression antipode
- Degree-2 quadratic eigenanalysis

This convergence across independent methods strengthens robustness.

10.2 Rejection of Alternative Geometries

Explicit testing demonstrates that the dataset does not preferentially encode:

- A 31°E TPW shear-net geometry
- A $\sim 170°$E geomagnetic excursion rotation plane

The Frost anisotropy field therefore does not appear to reflect either previously proposed geometry.

The extracted orientation is intrinsic.

10.3 Alignment with 121°E Euler Meridian

The dominant quadrupole axis lies within $\sim 11°$ of the proposed 121°E Euler meridian at $\sim 1\%$ significance.

Two statistically independent harmonic modes converge on the same rotational geometry.

This does not establish mechanism.

It does establish a geometric constraint: the inner-core anisotropy field is organised in a manner consistent with a specific Earth-fixed meridional framework.

10.4 Interpretive Boundaries

Several limitations must be emphasised:

1. Harmonic dominance does not imply dynamical causation.
2. Alignment does not establish rotational forcing.
3. Sampling geometry, though tested, remains imperfect.
4. The SEISGLOB2 comparison is geometric rather than mechanistic.

Demonstrating spatial organisation is easier than demonstrating cause.

The present results establish orientation and statistical robustness. They do not prescribe physical interpretation.

11 Conclusion

Using a geometry-first analytical framework, we demonstrate that:

- The inner-core anisotropy field exhibits strong multi-scale spatial coherence.
- Approximately one-third of signed variance is explained by a degree-2 spherical harmonic.
- The dominant quadrupole axis lies near 111°E.
- This axis lies within $\sim 11^\circ$ of a proposed 121°E Euler meridian at $\sim 1\%$ significance.
- Independent dipole and amplitude PCA analyses converge on the same orientation.
- Mid-mantle shear-velocity structure exhibits geometric association with this orientation within the 900–1200 km depth interval.

The convergence of two independent harmonic modes on the same Earth-fixed rotational geometry provides a robust geometric constraint on large-scale inner-core anisotropy.

The results are kinematic and statistical.

They do not assert mechanism.

They do define orientation.

Acknowledgements

The author acknowledges open data access provided by Frost et al. (2021) and the SEISGLOB2 team, and the use of several large-language-model tools (including GPT-5.2, Grok-4.1, Nemotron, LLaMA/Scout, and Claude Sonnet 4.5) in supporting roles during the development of this work. These systems assisted with code drafting and debugging, editorial refinement, conceptual clarification, and

"red-teaming" of the analysis and interpretations (i.e., probing assumptions, testing alternative framings, and identifying potential weaknesses). All empirical analyses, statistical procedures, data processing, model implementation, and scientific interpretation were designed, executed, and validated directly by the author, and were not performed autonomously by any AI system.

References

Creager, K. C. (1992). Anisotropy of the inner core from differential travel times of the phases PKP and PKIKP. *Nature*, 356, 309–314.

Durand, S., Debayle, E., Ricard, Y., & Lambotte, S. (2017). Seismic evidence for a change in the large-scale tomographic pattern across the 670 km discontinuity. *Earth and Planetary Science Letters*, 479, 1–14.

Frost, D. A., Rost, S., & Romanowicz, B. (2021). Inner core anisotropy from differential PKP travel times. *Journal of Geophysical Research: Solid Earth*, 126, e2020JB020866.

Silver, P. G. (1996). Seismic anisotropy beneath the continents: Probing the depths of geology. *Annual Review of Earth and Planetary Sciences*, 24, 385–432.

Tanaka, S., & Hamaguchi, H. (2002). Degree-one heterogeneity and hemispherical variation of anisotropy in the inner core. *Journal of Geophysical Research*, 107(B2), 2038.

Cunningham, R. (2024, May 23). *Master Exothermic Core-Mantle Decoupling – Dzhanibekov Oscillation (ECDO) Theory.* The Ethical Skeptic. Retrieved from `https://theethicalskeptic.com/2024/05/23/master-exothermic-core-mantle-decoupling-dzhanibekov-oscillation-theory/`